Anomalous spin dynamics in the coupled spin tetramer system $CuSeO_3$

S. Lee,[1] W.-J. Lee,[1] J. van Tol,[2] P. L. Kuhns,[2] A. P. Reyes,[2] H. Berger,[3] and K.-Y. Choi[1,*]

[1]*Department of Physics, Chung-Ang University, 84 Heukseok-ro, Seoul 156-756, Republic of Korea*

[2]*National High Magnetic Field Laboratory, Florida State University, Tallahassee, Florida 32310, USA*

[3]*Institute of Condensed Matter Physics, EPFL, CH-1015 Lausanne, Switzerland*

(Received 4 November 2016; revised manuscript received 16 December 2016; published 2 February 2017)

We report high-field magnetization, high-frequency electron spin resonance (ESR), and ^{77}Se nuclear magnetic resonance (NMR) measurements on the linear spin tetramer system $CuSeO_3$, consisting of strongly interacting Cu(1) dimers and weakly coupled Cu(2) spins. The magnetization exhibits anisotropic half-step magnetization plateaus at $\mu_0 H = 45$ T, depending on a crystallographic orientation. A temperature dependence of the ESR linewidth ΔH_{pp} in a paramagnetic phase points towards the significance of anisotropic exchange interactions. Below $T_N = 9$–10 K long-range magnetic order is evidenced by the observation of a critical divergence of both $\Delta H_{pp}(T)$ and the nuclear spin-lattice relaxation rate $1/T_1$. In addition, we identify a magnetic anomaly at $T^* = 6.0(5)$ K below T_N, which is caused by a spin reorientation. The nuclear spin-spin relaxation rate $1/T_2$ unveils the development of site-specific spin correlations. The intriguing magnetism of $CuSeO_3$ is discussed in terms of the energy hierarchy of Cu(1) and Cu(2) spins in concert with additional intertetramer interactions.

DOI: 10.1103/PhysRevB.95.054405

I. INTRODUCTION

Coupled spin clusters have attracted a great deal of theoretical and experimental interest owing to their fascinating phenomena arising from a crossover from zero-dimensional quantum to three-dimensional (3D) collective magnetism. The ground state of isolated antiferromagnetic spin clusters is given by either a spin singlet or a spin triplet state [1,2]. Applying an external field or pressure, on the one hand, can induce long-range magnetic order [3–13]. On the other hand, intercluster interactions can render the discrete energy level of an isolated cluster to form an energy band. If the spin gap is not bigger than the energy of the effective intercluster interaction, an ordered state can be generated by mixing different energy states. In the vicinity of a quantum critical regime from an ordered side, gapless Nambu-Goldstone modes coexist with a massive Higgs mode [14].

Among the coupled spin clusters, spin tetramers (four spin systems) have proved to be a versatile platform to explore an interplay between the isolated and collective magnetism. In accordance with the connectivity of four spins, the spin tetramer system can be classified into four different types of tetrahedral, square, diamond, and linear tetramers [15]. The present study will focus on the linear spin tetramer system comprising two intratetramer interactions: one is an exchange interaction J_{11} between the central pair spins and the other is an exchange interaction J_{12} between the edge and central spins as sketched in Fig. 1(a). The ratio J_{12}/J_{11} determines the nature of a ground state. For instance, $((CH_3)_3NH)_2Cu_4Br_{10}$, $SrCu_2(PO_4)_2$ and $PbCu_2(PO_4)_2$ with $J_{12}/J_{11} > 1.1$ display a spin-singlet ground state [16–18]. These compounds having negligible intertetramer interactions are in the spin-gap side but very few materials are so far known to be in the long-range ordered side. As such, little is understood about magnetic behaviors near a quantum critical point in a class of coupled linear tetramers.

$CuSeO_3$ is regarded as a prime candidate for the coupled tetramer system, which is placed in the magnetically ordered side [19,20]. $CuSeO_3$ has a monoclinic $P2_1/n$ crystal structure with two inequivalent Cu(1) and Cu(2) sites [21]. The distance between the apical O and Cu atoms (∼2.35 Å) is much longer than that of the planar O and Cu atoms (∼2.02 Å). On that account, the exchange interaction via the apical O atoms can be neglected to a first approximation [19]. When considering the dominant exchange paths through the $d_{x^2-y^2}$ orbitals, the magnetic lattice of $CuSeO_3$ consists of isolated Cu(2)-Cu(1)-Cu(1)-Cu(2) tetramers, running along the a axis [see Fig. 1(b)]. The intratetramer exchange interactions are estimated to be $J_{11} = 225$ K between the two central pair Cu(1) spins connected by edge sharing of two CuO_4 squares and $J_{12} = 160$ K between the two neighboring Cu(1) and Cu(2) spins [19]. The intertetramer interaction J_{22} is much smaller than both J_{11} and J_{12} due to the longer exchange paths through the apical O atoms. Noticeably, there are two orientations of the linear tetramers which are transformed into each other by a 180° rotation about the b axis. These tetramer chains are layer-by-layer stacked along the c axis, leading to a very small interchain interaction. Nonetheless, this interchain interaction is responsible for the antiferromagnetic long-range ordering which sets in at $T_N = 8$ K [19,20].

Indeed, the isolated linear tetramer model fails to reproduce a steep increase of the magnetic susceptibility for temperatures below 70 K [20]. In addition, X-band ESR and torque magnetometry measurements revealed a rotation of the magnetic axes and a variation of the effective g factors with temperature [20]. These anomalies are interpreted in terms of the development of site-selective spin correlations as well as of the important role of anisotropic exchange interactions.

In this paper we employ high-field magnetization, ESR, and ^{77}Se NMR measurements to clarify the underlying mechanism of anomalous spin dynamics reported in $CuSeO_3$. The high-field magnetization and ESR data point towards the significance of anisotropic exchange interactions. Both ESR and ^{77}Se NMR data evidence the presence of a magnetic anomaly at $T^* = 6$ K and the development of site-specific spin

*kchoi@cau.ac.kr

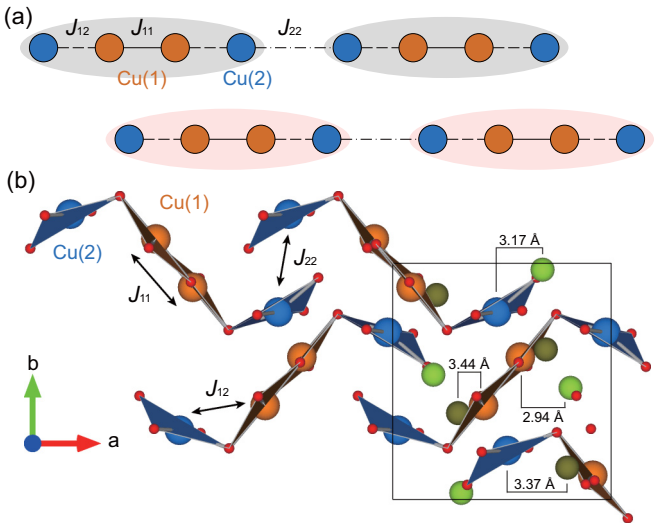

FIG. 1. (a) Schematic of coupled linear tetramers formed by the two intratetramer interactions J_{11} and J_{12} and one intertetramer interaction J_{22}. The shaded ovals indicate two differently oriented tetramers. (b) The spin tetramer of $CuSeO_3$ viewed along the c axis. The unit cell is drawn by the solid rectangle. The orange, blue, light green, olive, and red spheres represent the Cu(1), Cu(2), Se(1), Se(2), and O atoms, respectively. The distances of Cu(1)-Se(1), Cu(1)-Se(2), Cu(2)-Se(1), and Cu(2)-Se(2) are 2.94, 3.44, 3.17, and 3.37 Å, respectively.

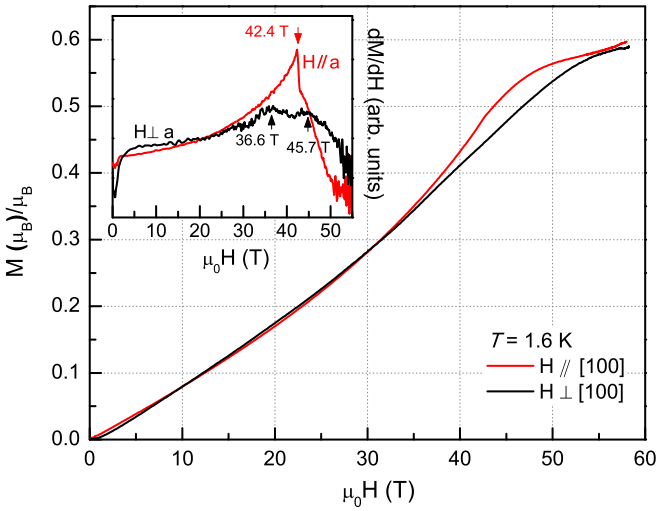

FIG. 2. The high-field magnetization curve $M(H)$ of $CuSeO_3$ measured for $\mu_0 H \| a$ and $\mu_0 H \perp a$ at $T = 1.6$ K. The inset plots the field derivative of $M(H)/dH$ for each direction.

correlations. These complex magnetic behaviors are ascribed to a large difference of the exchange energy between Cu(1) and Cu(2) spins, magnon-phonon coupling, and additional intertetramer interactions.

II. EXPERIMENTAL DETAILS

Single crystals of $CuSeO_3$ were prepared by a standard chemical vapor transport as described in Ref. [19]. High-field magnetization experiments at $T = 1.6$ K were conducted at Dresden High Magnetic Field Laboratory using a pulsed field magnet (20 ms duration) and an induction method with a pick-up coil device in the field range of $\mu_0 H = 0$–60 T.

For ESR measurements, a single crystal of $CuSeO_3$ was aligned along the [100] crystallographic direction. High-frequency ESR experiments were performed at $\nu = 240$ GHz with a heterodyne quasioptical spectrometer and sweepable 12.5 T superconducting magnet in the temperature range $T =$ 2–290 K [22]. The field derivative of a microwave absorption signal was recorded while sweeping an external field. ^{77}Se ($I = 1/2$, $\gamma_N = 8.13$ MHz/T) NMR spectra were obtained using a locally developed NMR spectrometer at National High Field Laboratory equipped with a high-homogeneity 17 T field-varying magnet. The temperature and angle dependence of ^{77}Se NMR spectra were taken by fast Fourier transform (FFT) of the NMR echo signal while sweeping the field at a fixed frequency $\nu = 81.48$ MHz. The single crystal was mounted on a goniometer for angular dependence measurements. The nuclear spin-lattice (spin-spin) relaxation time T_1 (T_2) was measured by a modified inversion recovery (Hahn pulse) method with pulse width $\pi/2 = 1$ μs in the temperature range of $T = 2.4$–250 K.

III. RESULTS

A. High-field magnetization

Figure 2 presents the high-field magnetization curve $M(H)$ of $CuSeO_3$ measured at 1.6 K for a magnetic field applied parallel and perpendicular to the a axis. The magnetization increases monotonically with increasing field and then saturates towards a half-magnetization plateau. In order to clarify the magnetization process, we take the field derivative of $M(H)$ as plotted in the inset of Fig. 2. We identify a single peak at $\mu_0 H = 42.4$ T for $\mu_0 H \| a$ and two peaks at $\mu_0 H = 36.6$ and 45.7 T for $\mu_0 H \perp a$, showing the different field positions of the half-magnetization plateau. The full saturation field is expected to occur at $\mu_0 H_S = k_B J_{11}/g\mu_B \approx 152$ T, which is not reachable with a nondestructive pulse magnet.

A close inspection further uncovers the bifurcation of $M(H)$ between the two crystallographic orientations for fields above 33 T. For $\mu_0 H \| a$, the magnetization displays a steep increase with an S-shape curvature, typical for a spin chain. This is in stark contrast to a gradual increase for $\mu_0 H \perp a$. The orientation-dependent magnetic behavior is also observed in the temperature dependence of magnetic susceptibility anisotropy [19]. This indicates the significant role of anisotropic exchange interactions and ferromagnetic interactions. We recall that the half-step magnetization plateau was observed in the coupled square tetramer $CdCu_2(BO_3)_2$ with $T_N = 9.8$ K that is composed of strongly interacting Cu(1) dimers and weakly coupled Cu(2) spins [23]. Applying an external magnetic field, the weakly coupled Cu(2) spins are easily polarized, leading to a large contribution to the magnetization while the Cu(1) dimers retain a singlet state, giving a negligible contribution to the magnetization [24,25]. Similar to $CdCu_2(BO_3)_2$, the Cu(2) spins are weakly coupled to the Cu(1) dimer in $CuSeO_3$ [19]. Thus, the site-selective magnetization process may occur in the two subsystems as a function of field.

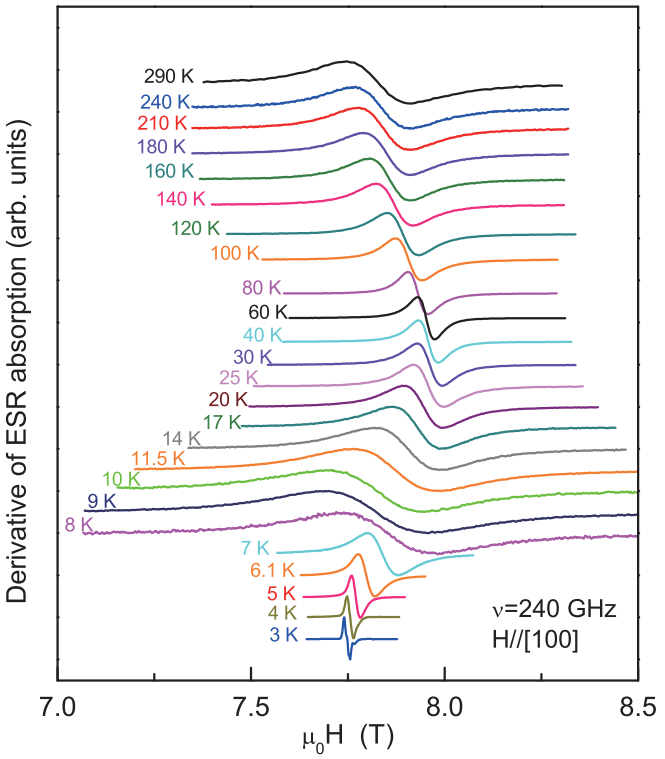

FIG. 3. Derivative of the ESR absorption spectra for $CuSeO_3$ measured for $\mu_0 H \| a$ at various temperatures. The spectra are vertically shifted for clarity and are normalized.

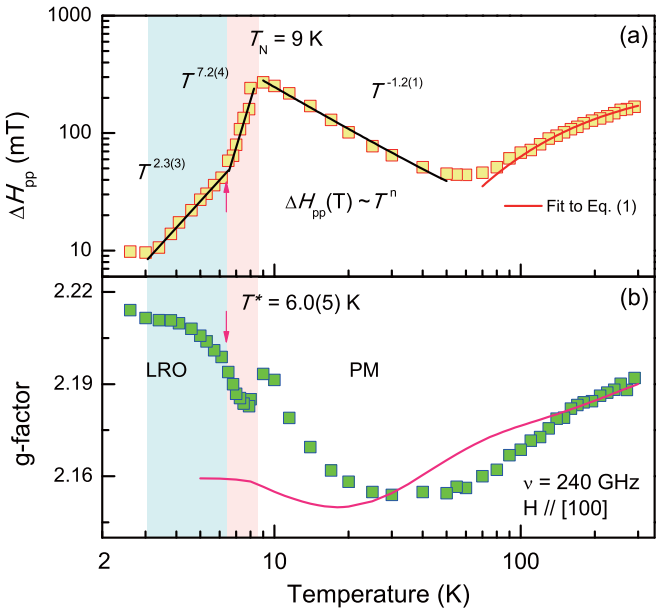

FIG. 4. Temperature dependence of (a) the peak-to-peak linewidth ΔH_{pp} on a log-log scale and (b) the g factor plotted along with the scaled bulk magnetic susceptibility (pink solid line) in a semilog scale. The black solid lines are a fit to a power law with the exponents $n = -1.2(1)$, 7.2(4), and 2.3(3) in the three different temperature regimes. The red solid line represents the fitting using Eq. (1) as described in the text. The magnetic anomaly is discernible at $T^* = 6.0(5)$ K below T_N as marked by the arrow and the shadings with different colors.

B. Electron spin resonance

We performed high-frequency ESR measurements at $\nu = 240$ GHz for $\mu_0 H \| a$. As shown in Fig. 3, the ESR spectra display an intriguing temperature dependence in their resonance field and linewidth. Upon cooling from 290 down to 50 K, the spectra first narrow while shifting to higher magnetic fields and then experience a critical-like broadening accompanying a shift of the resonance position towards lower magnetic field upon approaching $T_N = 9$ K.

For a quantitative analysis of the ESR signals, they are fitted to a single Lorentzian profile down 6 K. We note that at temperatures below 6 K the line shape deviates from a single Lorentzian, which could be related to the strong absorption in the narrow line leading nonlinear and interference effects, as the sample size is of the order of the wavelength. The g factor and the peak-to-peak linewidth ΔH_{pp} extracted from the fitting are plotted as a function of temperature in Fig. 4.

With decreasing temperature, both $\Delta H_{pp}(T)$ and the g factor decrease gradually, forming the minimum around 50 K. For $9 < T < 45$ K, the drastic ESR line broadening is described by a power law $\Delta H_{pp}(T) \sim (T - T_N)^{-1.2(1)}$. At the corresponding temperature range, the magnetic susceptibility deviates from the linear tetramer model. This together with the upward shift of the g factor is ascribed to the development of the intertetramer spin correlations with a subsequent growth of critical 3D correlations. When the temperature is lowered towards T_N, the critical broadening is given by $\Delta H_{pp}(T) \sim (T - T_N)^{-\alpha}$. We note that the observed critical exponent is not significantly different from the value of $\alpha = 1$ expected for the classical antiferromagnet.

For temperatures below T_N, we observe a sharp antiferromagnetic resonance (AFMR) mode. Upon cooling down from T_N, the AFMR signal significantly narrows. In classical 3D antiferromagnets without pronounced quantum fluctuations, the temperature dependence of the AFMR linewidth is determined by the population of magnons and follows a power law $\Delta H_{pp} \propto T^4$ [26]. We find that $CuSeO_3$ displays a weaker T dependence of $T^{2.3(3)}$ than the expected T^4 dependence for temperatures below $T^* = 6.0(5)$ K. Similar behavior has been reported in the frustrated magnets having the exponent of 1.4–2.2, implying persisting spin fluctuations [27–29]. Remarkably, the AFMR linewidth changes to a much stronger T-dependence $T^{7.2(4)}$ upon warming through T^*. At the respective temperature, the g factor steeply increases towards the saturation of $g = 2.21$. This suggests that the magnetic anomaly at T^* is due to a spin reorientation. This assertion is supported by the torque magnetometry measurements, which show a rotation of the magnetic easy axis by 3° in the ac plane down to 4 K [20].

Next, we turn our attention to $\Delta H_{pp}(T)$ in the paramagnetic phase of $50 < T < 300$ K. Normally, the decreasing $\Delta H_{pp}(T)$ with decreasing temperature originates from spin-phonon interactions or anisotropic exchange interactions. As our system shows no indication of structural instabilities, the spin-phonon mechanism is excluded as a possible origin. We recall that the T-linear decrease of the ESR linewidth with temperature is generic to spin chains or spin-ladder materials [30,31].

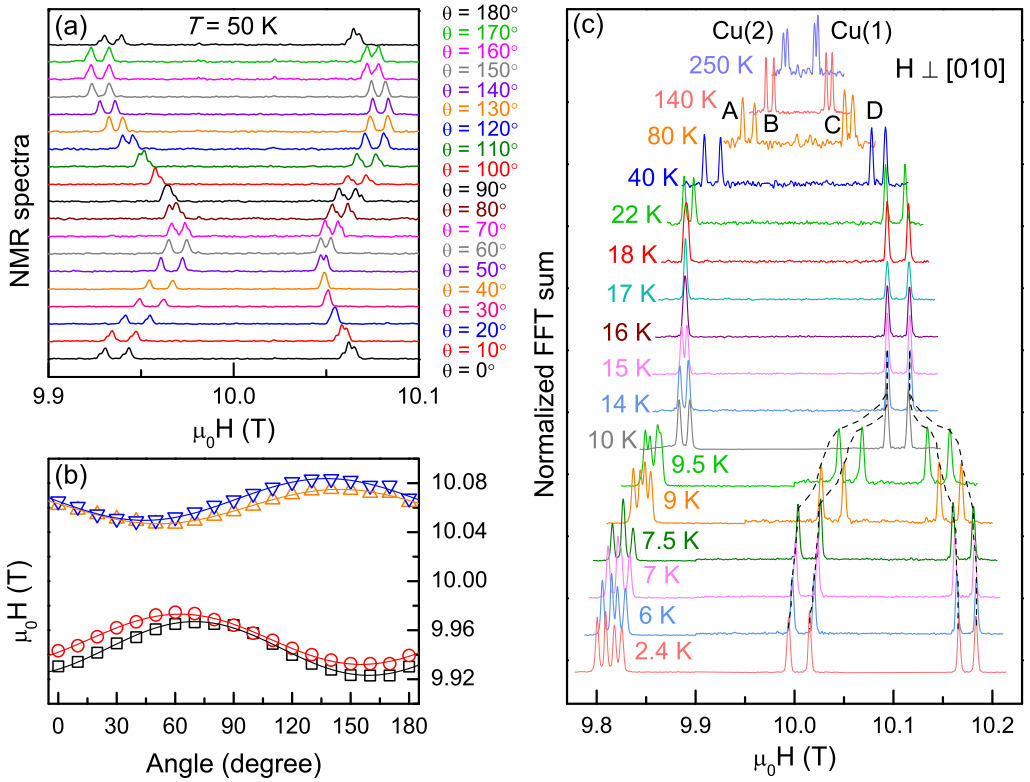

FIG. 5. (a) Angular dependence of the ^{77}Se NMR spectra measured at $T = 50$ K. (b) Angular dependence of the resonance field. Solid lines represent a fit to a sinusoidal function (see the main text). (c) Field-swept ^{77}Se NMR spectra of $CuSeO_3$ for $\mu_0 H \perp b$ obtained by integrating spin-echo intensity as a function of temperature. Peaks A and D are used for the relaxation measurements.

However, the Oshikawa and Affleck model is not applicable to the coupled spin tetramer system $SeCuO_3$. Noticeably, the high-temperature $\Delta H_{pp}(T)$ of the spin-Peierls compound $CuGeO_3$ features a strong decrease of the linewidth as the temperature is decreased while forming a broad minimum. This behavior is described by an empirical expression [19,32]

$$\Delta H_{SAE}(T) = \Delta H_{SAE}(\infty) e^{-\frac{C_1}{C_2+T}}. \quad (1)$$

Here the parameter C_1 corresponds to the isotropic exchange coupling constant J and C_2 is related to the Néel temperature T_N. This model accounts for the contribution of the symmetric anisotropic exchange interaction (SAE) to ΔH_{pp} in low-dimensional spin systems. We made an attempt to analyze the high-T ΔH_{pp} of $SeCuO_3$ in terms of Eq. (1) and found that this model fails to reproduce the $\Delta H_{pp}(T)$ data over the entire paramagnetic phase. Fixing the value of $C_2 = T_N$, we were able to reach a reasonable agreement between the fitted and experimental data for temperatures above 120 K, yielding $C_1 = 157 \pm 4$ K. This value is comparable to both J_{11} and J_{12}. Assuming that the ESR linewidth is solely determined by the SAE interaction, the shift of the g factor is scaled with the bulk magnetic susceptibility. As compared in Fig. 4(b), the g factor and $\chi(T)$ scale to each other above 140 K, but the scaling breaks down for temperatures below 140 K. The small deviation seen below 120–140 K for both $\Delta H_{pp}(T)$ and the g factor may indicate the presence of an additional relaxation mechanism possibly due to Dzyaloshinskii-Moriya (DM) interaction, which is allowed for the Cu(1)-Cu(2) bonding geometry [20].

C. ^{77}Se nuclear magnetic resonance

As the ^{77}Se nucleus has nuclear spin $I = 1/2$, we expect a single spectral line for each inequivalent Se site. The $CuSeO_3$ crystal contains two inequivalent Cu(1) and Cu(2) sites as well as two inequivalent Se(1) and Se(2) sites, leading to four peaks for an arbitrary orientation with respect to the external magnetic field.

In an attempt to find the field direction where two Se sites become equivalent, we measured the angular dependence of the ^{77}Se NMR spectrum while rotating the sample about the b axis. Figure 5(a) displays the angular dependence of the field-swept ^{77}Se NMR spectra at a fixed frequency $\nu = 81.49$ MHz and at $T = 50$ K. As plotted in Fig. 5(b), the angular dependence is well described by a sinusoidal function $\mu_0 H(\theta) \propto \sin(\theta - \theta_0)$, where θ is the angle between H and the a axis. It is evident that the local symmetry axis of both Se sites is not along any of the crystalline axes because the sample is monoclinic. That is the reason why we choose to work at the field direction of $\mu_0 H \perp b$, where all four peaks are well separated from each other. We assign the lower-field double peak signals to selenium sites, both Se(1) and Se(2), that are closest to Cu(2) spin and similarly, the higher-field signals to those closest to Cu(1). This assignment was inferred from the spin-spin relaxation data shown in Fig. 8 (*vide infra*). We shall refer to these signals as "Cu(2)" and "Cu(1)" lines in the following discussions. The total hyperfine coupling constant at the Se(1) and Se(2) sites is generally the sum of transferred hyperfine A_{trans} and dipolar A_{dip} couplings produced by Cu^{2+} spins, i.e., $A_{hf} = zA_{trans} + A_{dip}$, where z is the number of

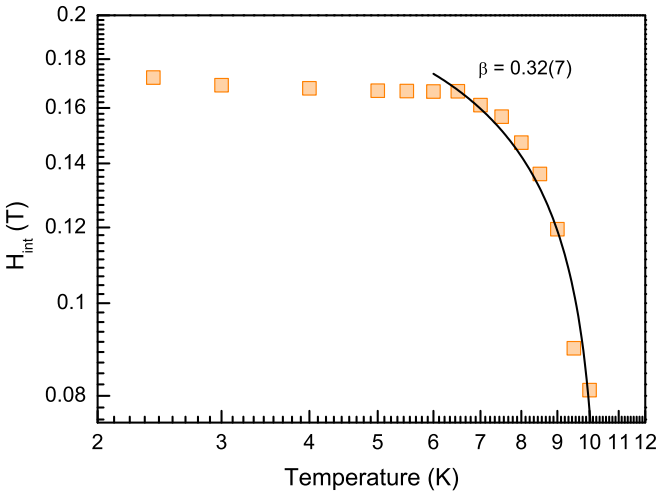

FIG. 6. Temperature dependence of the internal field $H_{\rm int}$ obtained from NMR spectra for $\mu_0 H \| b$ plotted in a log-log scale. The solid line is a fit to a power law.

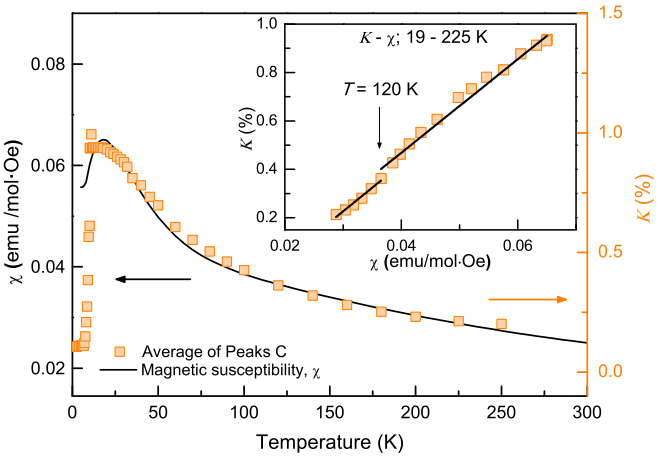

FIG. 7. Temperature dependencies of the magnetic shift K of ^{77}Se nuclear spins for peak C are shown together with the dc magnetic susceptibility χ measured using a SQUID magnetometer (black solid line). The inset shows K versus χ and the black solid lines are a fit to Eq. (2). A change of the slope is discernible at 120 K.

nearest-neighbor Cu^{2+} spins of each site. Here the transferred hyperfine couplings originate from Se($4p$)–O($2p$)–Cu($3d$) covalent bonds. Based on the opposite angular dependence of the higher- and the lower-field peaks, we conclude that the Cu(1) and Cu(2) spins produce the hyperfine field with opposite sign.

Figure 5(c) shows the field-swept NMR spectra in the temperature range of $T = 2.4$–250 K. As the temperature is lowered, the Cu(1) [Cu(2)] signal shifts towards higher (lower) fields. Below $T_{\rm N}$ each line was found to split into two lines. This is due to the development of the static internal field caused by a Néel type long-range ordering. The internal field $H_{\rm int}$, which is proportional to the Cu^{2+} sublattice magnetization, was determined from half the separation between the split lines. $H_{\rm int}$ versus T is plotted in Fig. 6 on a double logarithmic scale. To extract the critical exponent of the order parameter, $H_{\rm int}(T)$ is fitted by the power law $H_{\rm int}(T) \propto (1 - T/T_{\rm N})^{\beta}$. By restricting the fitting data points close to $T_{\rm N}$, we obtain $\beta = 0.32(7)$. This value is not significantly different from the critical exponent $\beta = 0.365$ expected for the 3D Heisenberg model. We further note that the correct value of the internal field is possibly higher than $H_{\rm int}$ because of the arbitrary direction that the data were taken but should not change the result.

The NMR shift provides a direct measure of the intrinsic spin susceptibility $\chi_{\rm spin}$. In Fig. 7 the temperature dependence of the magnetic shift $K_S(T)$ is plotted for peak C with the dc magnetic susceptibility measured at $\mu_0 H = 0.1$ T. We determine $A_{\rm hf}$ between the ^{77}Se nuclear and Cu^{2+} electronic spins through the Clogston-Jaccarino plot with temperature as an implicit parameter [33],

$$K_S(T) = K_{\rm chem} + \frac{A_{\rm hf}}{N_{\rm A}\mu_{\rm B}}\chi_{\rm spin}(T). \quad (2)$$

Here $K_{\rm chem}$ is a temperature-independent chemical or orbital shift and $N_{\rm A}$ is the Avogadro number. The K-χ plot is fitted well by straight lines. We find a breaking slope through 120 K. $A_{\rm hf}$ is listed in Table I in the two temperature intervals of 19–120 K and 120–225 K. Peak B shows the largest change of $A_{\rm hf}$, suggesting the site-specific variation of $A_{\rm hf}$, which is linked to the change of the effective g tensors with temperature.

In order to probe the low-energy spin excitations, the nuclear spin-lattice (spin-spin) relaxation rate $1/T_1$ ($1/T_2$) was measured in the temperature range $T = 2.4$–100 K. The two different lines A and D were selectively irradiated. In Fig. 8 the temperature dependence of $1/T_1$ and $1/T_2$ is shown on a double logarithmic scale. The temperature dependence of $1/T_1$ for the Cu(1) and Cu(2) spins is alike.

A sharp peak in $1/T_1$ versus T at 10 K is due to the phase transition from the paramagnetic state to the antiferromagnetically ordered state. The transition temperature is slightly higher than the zero-field value. This is associated with the suppression of quantum fluctuations in high fields, leading to the enhancement of the classical magnetic ordering. Above 15 K $1/T_1$ is largely temperature independent, typical for a spin-lattice relaxation process driven by the spin flips of the fast-fluctuating Cu^{2+} paramagnetic moments. In a short-correlation time $\omega\tau \ll 1$, $1/T_1$ is approximated as [34]

$$\frac{1}{T_1} \approx \frac{2}{5}\gamma^2 A^2 S(S+1)\tau, \quad (3)$$

where the gyromagnetic ratio of the ^{77}Se nuclei $\gamma_{\rm N} = 8.13 \times 10^{-6}$ s^{-1} T^{-1}, the hyperfine coupling constant $A_{\rm hf} = 0.2675$ T/$\mu_{\rm B}$, and the electron spin $S = 1/2$. With $1/T_1 = 235$ s^{-1}, the correlation time of the Cu^{2+} spins is estimated to be $\tau = 1.35 \times 10^{-9}$ s. We note that the critical line broadening probed by ESR starts at 45 K. Meanwhile, the critical behavior

TABLE I. Hyperfine coupling constant in a unit of T/μ_B for temperatures $T < 120$ K and $T > 120$ K.

	$A_{\rm hf}$ ($T < 120$ K)	$A_{\rm hf}$ ($T > 120$ K)
Peak A	0.2675	0.2624
Peak B	0.2758	0.2071
Peak C	0.1942	0.1952
Peak D	0.2446	0.2260

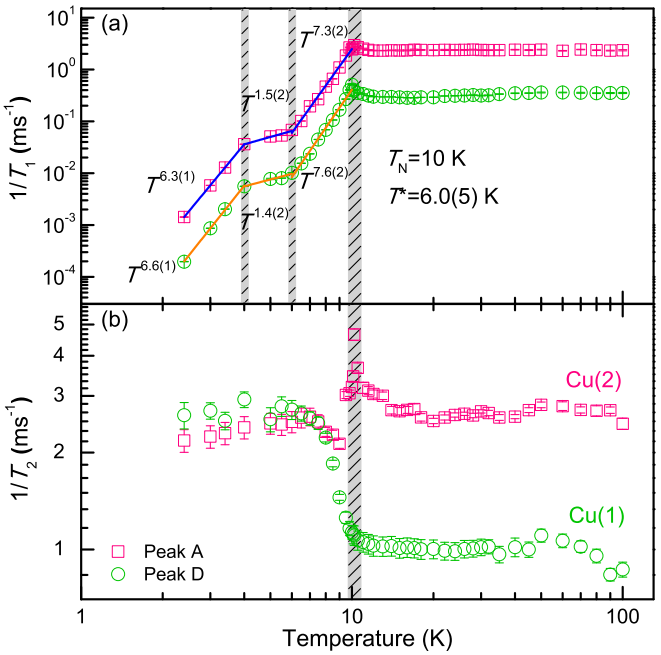

FIG. 8. Temperature dependence of (a) the nuclear spin-lattice relaxation rate $1/T_1$ and (b) the nuclear spin-spin relaxation rate $1/T_2$ in a log-log plot. In addition to the antiferromagnetic ordering at T_N, both $1/T_1$ and $1/T_2$ give a signature for a magnetic anomaly at $T^* = 6.0(5)$ K marked by the gray bars. The blue and orange solid lines are a fit to a power law.

of $1/T_1$ is observed below 15 K. This discrepancy is related to the fact that the ESR technique (hundred gigahertz time window) probes much faster spin fluctuations than the NMR technique (hundred megahertz).

In the antiferromagnetic ordered state, $1/T_1$ is governed by scattering of magnons off nuclear spins, yielding a power-law temperature dependence for $T \gg \Delta$ where Δ is the gap in spin waves. $1/T_1$ displays T^7-like behavior, except for the intermediate temperature interval ($4 < T < 6$ K). The T^7 dependence corresponds to the Raman process of mixed magnon-phonon modes [35]. The magnon-phonon coupling allows the phonons to induce magnetic relaxation processes. Indeed, the strong spin-lattice coupling is present in the ordered state [20]. The weaker $T^{1.5}$ dependence may be linked to the T^* magnetic anomaly observed in the ESR experiment.

We turn to the temperature dependence of $1/T_2$. Unlike $1/T_1$, $1/T_2$ shows a site-dependent behavior. Peaks A and B exhibit a clear divergence at T_N, confirming the transition to long-range magnetic order. This is in sharp contrast to peaks C and D showing a steep increase below 10 K and then a subsequent saturation below 6 K. This suggests the development of the site-specific spin correlations. As the Cu(1) spins are coupled by a strong dimer coupling, the Cu(1) spins are dominated by singlet correlations. On the other hand, the weakly coupled Cu(2) spins easily form a staggered magnetization. This gives a justification to the assignment of peaks A and B (C and D) to the Cu(2) [Cu(1)] line in Fig. 5(c).

IV. DISCUSSION AND SUMMARY

Combining magnetization with two resonance techniques, we have unveiled a number of anomalous magnetic behaviors in the linear tetramer system $CuSeO_3$. First, the magnetization curve displays the half-step magnetization plateaus around $\mu_0 H = 45$ T. The salient feature is the orientation dependence of the magnetization slope for fields above 33 T. Second, the increasing $\Delta H_{pp}(T)$ with temperature in a paramagnetic regime indicates the presence of two kinds of the SAE and DM interactions. Third, the hyperfine coupling constant exhibits the site-specific variation through 120 K. Fourth, in the ordered phase both $1/T_1$ and the AFMR linewidth provide a spectroscopic signature of a magnetic anomaly at $T^* = 6.0(5)$ K, arising from a spin reordering. Finally, the nuclear spin-lattice relaxation process is governed by magnon-phonon coupling and the nuclear spin-spin relaxation shows a distinct evolution of spin correlations between the Cu(1) and Cu(2) spins.

All these data signify the anisotropic exchange interactions and the additional exchange interactions beyond the J_{11}-J_{12}-J_{22} coupled linear tetramer model. On the one hand, the superexchange paths through the CuO_4 distorted square lead to the intratetramer interactions J_{11} and J_{12}. On the other hand, the apical oxygens give a route to the Cu-O-Cu superexchange paths, giving rise to the weak intertetramer interaction J_{22}. The J_{11}-J_{12}-J_{22} model constitutes an alternating spin chain along the a axis. In addition, the interchain interactions should be evoked to explain a long-range magnetic order. Furthermore, the ferromagnetic intertetramer interaction may be present, on the basis of the steep increase of the magnetic susceptibility below 70 K. For the precise determination of a full spin Hamiltonian, future works on *ab initio* calculations are called for.

A combined effect of the spin-phonon coupling and the CuO_6 octahedral distortions can account for the site-specific variation of the hyperfine coupling constant and the rotation of the magnetic moments in the ordered state. The site-specific spin correlations may be explained by considering the energy hierarchy $J_{11} > J_{12} \gg J_{22}$, forming the two subsystems made of the strongly coupled Cu(1) dimers and the weakly coupled Cu(2) spins. In this case, the Cu(1) ordered magnetic moments will be smaller than the Cu(2) one due to pronounced singlet fluctuations as seen from the lacking divergence of $1/T_2$ at T_N for the Cu(2) spins. In addition, we expect that the ordered moments of the Cu(1) and Cu(2) spins evolve in a different manner with increasing magnetic field. Neutron diffraction measurements are requested to examine this intriguing scenario on the magnetic ordering and magnetization processes.

In summary, we have presented high-field magnetization, ESR, and ^{77}Se NMR measurements of the linear tetramer system $CuSeO_3$. We find experimental signatures for a spin reordering, site-specific spin correlations, and anisotropic magnetization process. Our study demonstrates that small perturbations can exert a strong impact on low-energy magnetic behaviors in a class of coupled tetramer systems which has a large difference in the involved magnetic energy.

ACKNOWLEDGMENTS

This work was supported by the Korea Research Foundation (KRF) grant funded by the Korea government (MEST) (Grants No. 2009-0076079 and No. 2016-911392). This research was

supported by the Chung-Ang University Excellent Student Scholarship in 2015. The National High Magnetic Field Laboratory is supported by NSF Cooperative Agreement No. DMR-1157490, and by the State of Florida.

[1] D. Gatteschi, R. Sessoli, and J. Villain, *Molecular Nanomagnets* (Oxford University Press, New York, 2006).
[2] K.-Y. Choi, Y. H. Matsuda, H. Nojiri, U. Kortz, F. Hussain, A. C. Stowe, C. Ramsey, and N. S. Dalal, Phys. Rev. Lett. **96**, 107202 (2006).
[3] S. Sachdev, *Quantum Phase Transitions* (Cambridge University Press, Cambridge, 1999).
[4] N. Cavadini, Ch. Rüegg, A. Furrer, H.-U. Güdel, K. Krämer, H. Mutka, and P. Vorderwisch, Phys. Rev. B **65**, 132415 (2002).
[5] Ch. Rüegg, N. Cavadini, A. Furrer, H.-U. Güdel, K. Krämer, H. Mutka, A. Wildes, K. Habicht, and P. Vorderwisch, Nature (London) **423**, 62 (2003).
[6] H. Kageyama, M. Nishi, N. Aso, K. Onizuka, T. Yosihama, K. Nukui, K. Kodama, K. Kakurai, and Y. Ueda, Phys. Rev. Lett. **84**, 5876 (2000).
[7] K. Kodama, M. Takigawa, M. Horvatić, C. Berthier, H. Kageyama, Y. Ueda, S. Miyahara, F. Becca, and F. Mila, Science **298**, 395 (2002).
[8] P. Lemmens, K.-Y. Choi, E. E. Kaul, C. Geibel, K. Becker, W. Brenig, R. Valenti, C. Gros, M. Johnsson, P. Millet, and F. Mila, Phys. Rev. Lett. **87**, 227201 (2001).
[9] K. Totsuka and H.-J. Mikeska, Phys. Rev. B **66**, 054435 (2002).
[10] W. Brenig, Phys. Rev. B **67**, 064402 (2003).
[11] K. Prša, H. M. Rønnow, O. Zaharko, N. B. Christensen, J. Jensen, J. Chang, S. Streule, M. Jiménez-Ruiz, H. Berger, M. Prester, and J. Mesot, Phys. Rev. Lett. **102**, 177202 (2009).
[12] K.-Y. Choi, H. Nojiri, N. S. Dalal, H. Berger, W. Brenig, and P. Lemmens, Phys. Rev. B **79**, 024416 (2009).
[13] K.-Y. Choi, S. H. Do, P. Lemmens, J. van Tol, J. Shin, G. S. Jeon, Y. Skourski, J.-S. Rhyee, and H. Berger, Phys. Rev. B **90**, 184402 (2014).
[14] P. Merchant, B. Normand, K. W. Krämer, M. Boehm, D. F. McMorrow, and Ch. Rüegg, Nat. Phys. **10**, 373 (2014).
[15] S. Emori, T. Tokii, and Y. Muto, Bull. Chem. Soc. Jpn. **48**, 1649 (1975).
[16] U. Geiser, R. D. Willett, M. Lindbeck, and K. Emerson, J. Am. Chem. Soc. **108**, 1173 (1986).
[17] A. A. Belik, M. Azuma, A. Matsuo, M.-H. Whangbo, H.-J. Koo, J. Kikuchi, T. Kaji, S. Okubo, H. Ohta, K. Kindo, and M. Takano, Inorg. Chem. **44**, 6632 (2005)
[18] A. A. Belik, M. Azuma, A. Matsuo, T. Kaji, S. Okubo, H. Ohta, K. Kindo, and M. Takano, Phys. Rev. B **73**, 024429 (2006).
[19] I. Živković, D. M. Djokić, M. Herak, D. Pajić, K. Prša, P. Pattison, D. Dominko, Z. Micković, D. Cinčić, L. Forró, H. Berger, and H. M. Rønnow, Phys. Rev. B **86**, 054405 (2012).
[20] M. Herak, A. G. Čabo, D. Žilić, B. Rakvin, K. Salamon, O. Milat, and H. Berger, Phys. Rev. B **89**, 184411 (2014).
[21] H. Effenberger, Z. Kristallogr. **175**, 61 (1986).
[22] G. W. Morley, L. C. Brunel, and J. van Tol, Rev. Sci. Instrum. **79**, 064703 (2008); J. van Tol, L. C. Brunel, and R. J. Wylde, *ibid.* **76**, 074101 (2005).
[23] M. Hase, M. Kohno, H. Kitazawa, O. Suzuki, K. Ozawa, G. Kido, M. Imai, and X. Hu, Phys. Rev. B **72**, 172412 (2005).
[24] O. Janson, I. Rousochatzakis, A. A. Tsirlin, J. Richter, Yu. Skourski, and H. Rosner, Phys. Rev. B **85**, 064404 (2012).
[25] W.-J. Lee, S.-H. Do, S. Yoon, Z. H. Jang, B. J. Suh, J. H. Lee, A. P. Reyes, P. L. Kuhns, H. Luetkens, and K.-Y. Choi, Phys. Rev. B **90**, 214416 (2014).
[26] S. M. Rezende and R. M. White, Phys. Rev. B **14**, 2939 (1976).
[27] K.-Y. Choi, Z. Wang, A. Ozarowski, J. van Tol, H. D. Zhou, C. R. Wiebe, Y. Skourski, and N. S. Dalal, J. Phys.: Condens. Matter **24**, 246001 (2012).
[28] D. Wulferding, K.-Y. Choi, P. Lemmens, A. N. Ponomaryov, J. van Tol, A. T. M. N. Islam, S. Toth, and B. Lake, J. Phys.: Condens. Matter **24**, 435604 (2012).
[29] K.-Y. Choi, I. H. Choi, P. Lemmens, J. van Tol, and H. Berger, J. Phys.: Condens. Matter **26**, 086001 (2014).
[30] M. Oshikawa and I. Affleck, Phys. Rev. B **65**, 134410 (2002).
[31] A. N. Ponomaryov, M. Ozerov, L. Zviagina, J. Wosnitza, K. Yu. Povarov, F. Xiao, A. Zheludev, C. Landee, E. Čižmár, A. A. Zvyagin, and S. A. Zvyagin, Phys. Rev. B **93**, 134416 (2016).
[32] R. M. Eremina, M. V. Eremin, V. N. Glazkov, H.-A. Krug von Nidda, and A. Loidl, Phys. Rev. B. **68**, 014417 (2003).
[33] R. Nath, Y. Furukawa, F. Borsa, E. E. Kaul, M. Baenitz, C. Geibel, and D. C. Johnston, Phys. Rev. B **80**, 214430 (2009).
[34] A. Abragam, *Principles of Magnetic Resonance* (Oxford Science, Oxford, 1960).
[35] P. Pincus and J. Winter, Phys. Rev. Lett. **7**, 269 (1961).